Double balanced differential configuration for high speed InGaAs/InP single photon detector at telecommunication wavelengths*

ZHENG Fu (郑福)[1,2], **ZHU Ge** (朱阁)[1,3], **LIU Xue-feng** (刘雪峰)[1], **WANG Chao** (王超)[1,3], **SUN Zhi-bin** (孙志斌)[1], **and ZHAI Guang-jie** (翟光杰)[1]**

1. Key Laboratory of Electronics and Information Technology for Space Systems, Center for Space Sciences and Applied Research, Chinese Academy of Sciences, Beijing 100190, China

2. University of Chinese Academy of Sciences, Beijing 100049, China

3. College of Physics, Beijing Institute of Technology, Beijing 100081, China

(Received 15 November 2014)

In this paper, we present an innovative method of double balanced differential configuration, in which two adjacent single photon avalanche diodes (SPADs) from the same wafer are configured as the first balanced structure, and the output signal from the first balanced stage is subtracted by the attenuated gate driving signal as the second balanced stage. The compact device is cooled down to 236 K to be characterized. At a gate repetition rate of 400 MHz and a 1 550 nm laser repetition rate of 10 MHz, the maximum photon detection efficiency of 13.5% can be achieved. The dark count rate is about 10^{-4} ns^{-1} at photon detection efficiency of 10%. The afterpulsing probability decreases with time exponentially. It is shown that this configuration is effective to discriminate the ultra-weak avalanche signal in high speed gating rates.

Document code: A **Article ID:** 1673-1905(2015)02-0121-4

DOI 10.1007/s11801-015-4213-0

Single-photon detectors have a wide application range, including quantum key distribution (QKD), optical time domain reflectometry (OTDR), integrated circuit testing, light detection and ranging (LIDAR), three dimensional LADAR imaging and fluorescence lifetime imaging[1]. Among them, one of the most demanding applications is QKD[2], which requires low noise, high efficiency and high speed[3]. High speed InGaAs/InP single photon detectors[4] at telecommunication wavelengths have developed widely in recent years. Afterpulsing is the main limit to the detection rate, so the narrow gates are usually applied to decrease the avalanche time to reduce the charge flow during the avalanche, thus afterpulsing effect can be alleviated. However, when the gate width is reduced, the avalanche signal is so weak that it's always buried in the capacitive transients resulting from the junction capacitance, which makes it hard to be discriminated. Capacitive spike noise has been problematic in high speed InGaAs/InP single photon detection applications. Different techniques, such as delay line matching[5], self-differencing[6,7], sine-wave gating[8], time-to-voltage converter[9], Gaussian pulse[10] and harmonics[11] gating techniques, have been employed to cancel the parasitic capacitive transients. Delay line matching and self-differencing usually can only work at a fixed frequency, because it is difficult to tune the coaxial cable length. In addition, self-differencing potentially limits the detection rate to the half of its gating rates[12]. More seriously, the intrinsic imperfection of self-differencing single-photon detector harms the security of high-speed quantum cryptography systems[13].

Balanced avalanche photodiodes (APDs), which have the potential detection rate up to gate repetition rate, have also been developed to overcome such drawbacks. A matched capacitor was used to reproduce the spurious peaks[14]. Wu[15] and Zhang[16] respectively employed a diode to subtract the capacitive transients from the signal. Besides, two commercially discrete single photon avalanche diodes (SPADs) were investigated[17,18]. In Refs.[19] and [20], two adjacent APDs in the same wafer were used in the balanced configuration, and the excellent matching is obtained. However, it needs two opposite polar gate signals.

In this paper, we present a double balanced differential configuration together with integrated dual SPADs with active area diameter of 200 μm, which are adjacent to the

* This work has been supported by the National Key Scientific Instrument and Equipment Development Project of China (No.2013YQ030595), the National High Technology Research and Development Program of China (No.2013AA122902), the National Natural Science Foundation of China (No.61274024) and National Natural Science Foundation of China for the Youth (No.40804032).

** E-mail：gjzhai@nssc.ac.cn

same wafer. The output signal is first subtracted by another blanked APD output signal, and then it is subtracted by the attenuated gate driving signal. The APDs and cooler are integrated in the same package, which can be cooled together to 236 K. Then we investigate its common mode cancellation result with this double balanced differential configuration.

We fabricate a compact device with dual APDs in a small package of TO-8. The widely used separate absorption, charge and multiplication (SACM) structure[21] is adopted to fabricate these InGaAs/InP SPADs with diameter of 200 μm. The balanced dual APDs are located adjacently in the same wafer, so their parameters match well to a large extent. One of them is coupled with a single-mode fiber, and the other is blanked. And four resistors are also integrated in the package as shown in Fig.1, thus each APD is configured as gated passive quenching mode. The whole device is cooled down to –25 °C together by a Peltier cooler (RMT Ltd, 2MDX04-138-0816). And all of these together with a thermistor are integrated in the TO-8 package.

A double balanced differential configuration is developed as shown in Fig.1. The power of the 400 MHz sinusoidal gate signal is fixed at –3 dBm. Then it is amplified by 35 dB with ZHL-42W. The amplified signal is divided by the power splitter #1 (ZAPD-2-252+), and one of its output is sent to the power splitter #2. Then the two outputs of power splitter #2 are fed to the cathode of two APDs through capacitors, resulting in about 20 dBm gate wave at each APD, which is about 6.3 V_{pp}. The 180° power combiner #1 cancels the outputs of the dual APDs. To further suppress the residual noise of the balanced dual APDs, another balanced differential stage is introduced. One output from power splitter #1 is attenuated by EVA-1500+ and phase shifted by JSPHS-1000, and then subtracted from the 20 dB amplified differential avalanche signal by 180° power combiner #2. Finally, the signal is amplified by 20 dB with ZFL-1000LN+ and fed to a counter or a time-correlated single photon counting (TCSPC) module.

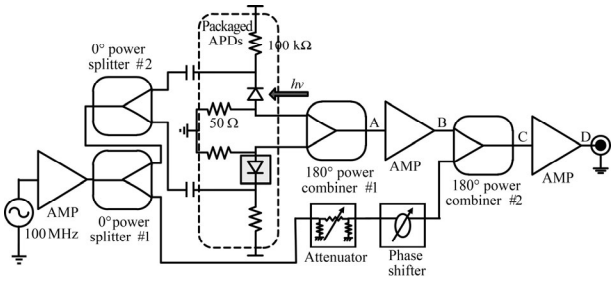

Fig.1 Schematic diagram of the double balanced differential configuration

The laser is synchronized with the gate signal at frequency of 10 MHz, which is $f_g/40$, where f_g is gate frequency. And a field programmable gate array (FPGA) board serves as the frequency divider and the delay generator. The pulse laser at 1 550 nm (id300, id Quantique) with full width at half maximum (FWHM) of 300 ps is attenuated to the single photon level of 0.1 photon per pulse by a calibrated variable attenuator.

When it is operated at high speed, the avalanche signal is rather small. Although the parameters of both APDs are highly consistent, there are about 30 mV residual noise left at node A, which is still so high that the avalanche signal can't be discriminated properly. After passing through another balanced differential stage and two stage amplifiers, the avalanche signal at node D is so high that it stands against the noise floor of about 10 mV, as shown in Fig.2.

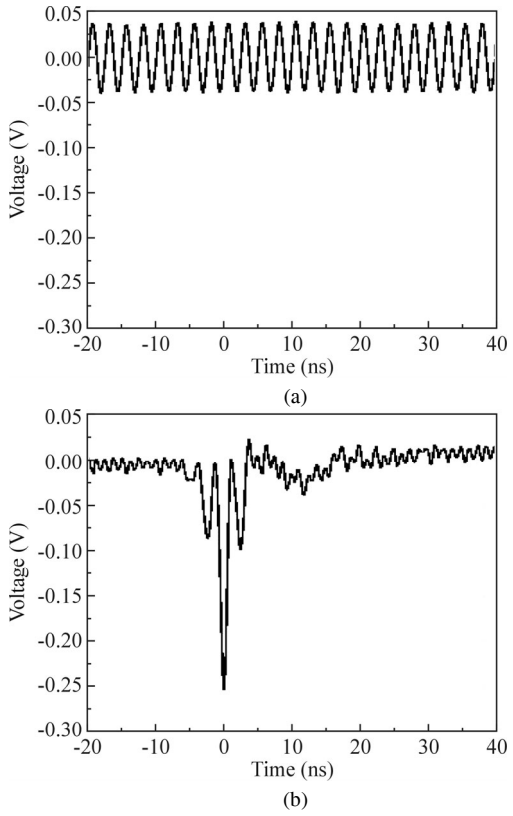

Fig.2 (a) Voltage at node A after the first balance cancellation stage; (b) Voltage at node D after the second balance cancellation stage

Photon detection efficiency (PDE), dark count rate (DCR) and afterpulsing probability are all important parameters to characterize single photon detectors[21]. We evaluate these parameters at 236 K, and the breakdown voltage of APD at this temperature is 55.6 V.

The output is connected with a TCSPC module (SPC-130), and measured over the range of 100 ns. We obtain the photon counts represented in counts per second (cps) as shown in Fig.3, from which we can extract the photon counts, dark counts and afterpulses. From Fig.3, we can see that the counts in the gates following the illuminated gate are rather large, and then the counts slowly decrease to nearly dark count level. The APD is

operated at PDE of 10%. The afterpulsing probability P_a can be calculated by

$$P_a = \frac{(C_{NI} - C_D)R}{C_I - C_{NI}}, \quad (1)$$

where C_{NI} and C_I are the average counts in the non-illuminated gates and the illuminated gates when the laser is turned on, C_D is the dark counts per gate with the laser completely off, and R is the ratio between gate repetition rate and laser rate. In our case, R is 40. The highest peak shown in the inset of Fig.3 represents the gate coinciding with the laser pulse, and it can be seen that the APD time jitter is about 350 ps at PDE of 10%.

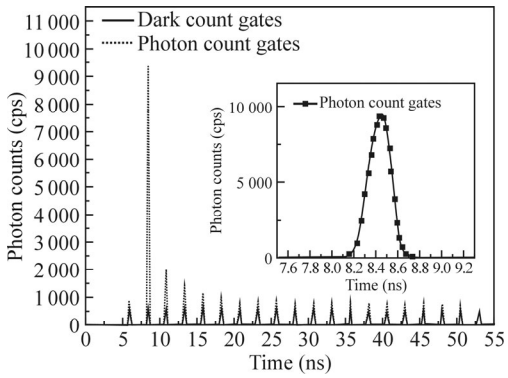

Fig.3 Photon counts collected by TCSPC module SPC-130 at PDE of 10% (The inset is the enlarged figure of the highest peak.)

PDE η and DCR R_{dc} can be expressed as

$$R_{dc} \times \tau_e = -\ln(1 - P_d), \quad (2)$$

$$\eta = \frac{1}{n}\ln\left(\frac{1 - P_d}{1 - P_t}\right), \quad (3)$$

where P_d and P_t are the probabilities of dark counts and total counts, respectively, and τ_e is the effective pulse width, which can be obtained by tuning the delay between laser and gates and measuring the FWHM of the temporal distribution of the photon counts in the illuminated gate shown in Fig.4. In our case, τ_e is 865 ps.

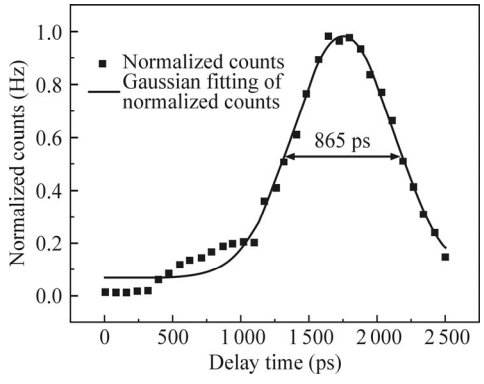

Fig.4 Temporal distribution of the photon counts

By adjusting the bias voltage, PDE and DCR as a function of overbias voltage are obtained as shown in Fig.5, where overbias voltage means the voltage at which the bias voltage is above breakdown voltage. It can be seen from Fig.5 that the DCR increases with the bias exponentially, and the PDE increases with the bias voltage. The DCR is rather large, and the PDE increases nonlinearly, which do not consist with the results demonstrated in traditional low speed detection[22]. The high DCR is caused by the large sensitive area and the temperature not low enough. The nonlinearity of PDE is probably caused by the dark count cancelation effect[19]. And at PDE of 10%, DCR is about 10^{-4} ns^{-1}, and the maximum PDE is about 13.5%.

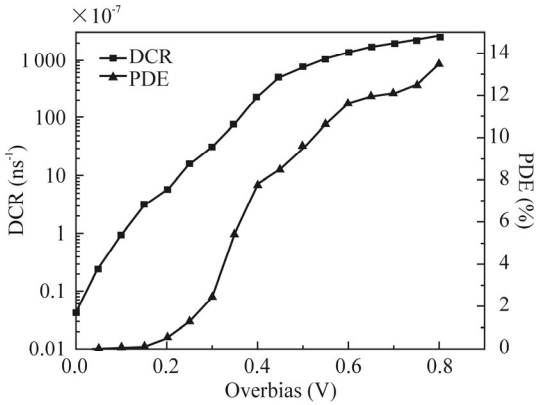

Fig.5 PDE and DCR as a function of overbias voltage

In Fig.6, we calculate the afterpulsing probability in the following gates with different times after laser pulse at PDE of 10%. We can see that the afterpulsing probability approximately follows an exponential decay principle, which can be dictated as

$$y = A \times \exp\left(-\frac{x}{\tau_{ap}}\right) + b, \quad (4)$$

where x represents time, y represents afterpulsing probability, A represents the coefficient of aftrepusling decay principle which is 25.709 3, and b is the offset which is 0.947 83. Most importantly, τ_{ap} is the aftrepusling decay time constant, which is 4.111 38 ns.

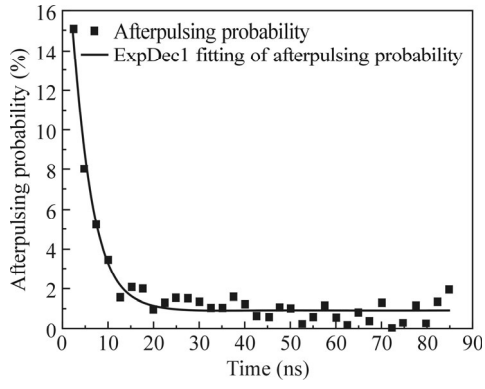

Fig.6 Afterpulsing probability distribution at PDE of 10%

We demonstrate a double balanced differential spike cancelling configuration with integrated dual SPADs. This method cancels the capacitive spike noise effectively to discriminate tiny avalanche signals in high speed gating rates. At a gate repetition of 400 MHz and a 1 550 nm laser repetition rate of 10 MHz, the photon detection efficiency of 13.5% can be achieved with dark count rate of 10^{-4} ns^{-1} at the temperature of 236 K. The afterpulsing probability decreases with time following an exponential decay principle. And the time jitter of the APD is about 350 ps at photon detection efficiency of 10%.

References

[1] M. Mazzillo, G. Condorelli, D. Sanfilippo, G. Fallica, E. Sciacca, S. Aurite, S. Lombardo, E. Rimini, M. Belluso, S. Billotta, G. Bonanno, A. Campisi, L. Cosentino, P. Finocchiaro, F. Musumeci, S. Privitera and S. Tudisco, Optoelectronics Letters **3**, 177 (2007).

[2] H.-Q. Ma, L. Wang, S. Li, R.-Z. Jiao and L. Wu, Optoelectronics Letters **8**, 318 (2012).

[3] H.-Q. Zhang, Y.-Y. Zhou, X.-J. Zhou and P.-G. Tian, Optoelectronics Letters **9**, 389 (2013).

[4] Z. Fu, W. Chao, S. Zhibin and Z. Guangjie,, Journal of Optoelectrnocs·Laser **25**, 1254 (2014). (in Chinese)

[5] D. S. Bethune and W. P. Risk, IEEE Journal of Quantum Electronics **36**, 340 (2000).

[6] Z. Yuan, B. Kardynal, A. Sharpe and A. Shields, Applied Physics Letters **91**, 041114 (2007).

[7] X. Chen, E. Wu, G. Wu and H. Zeng, Optics Express **18**, 7010 (2010).

[8] N. Namekata, S. Sasamori and S. Inoue, Optics Express **14**, 10043 (2006).

[9] A. Bouzid, A. M. Nahhas and K. Guedri, Optics Communications **328**, 37 (2014).

[10] Y. Zhang, X. Zhang and S. Wang, Optics Letters **38**, 606 (2013).

[11] A. Restelli, J. C. Bienfang and A. L. Migdall, Applied Physics Letters **102**, 141104 (2013).

[12] K. Patel, J. Dynes, A. Sharpe, Z. Yuan, R. Penty and A. Shields, Electronics Letters **48**, 111 (2012).

[13] M.-S. Jiang, S.-H. Sun, G.-Z. Tang, X.-C. Ma, C.-Y. Li and L.-M. Liang, Physical Review A **88**, 062335 (2013).

[14] A. Tosi, A. Della Frera, A. Bahgat Shehata and C. Scarcella, Review of Scientific Instruments **83**, 013104 (2012).

[15] G. Wu, C. Zhou, X. Chen and H. Zeng, Optics Communications **265**, 126 (2006).

[16] Y. Zhang, F. Xie, G. Yang, X. Zhang and S. Wang, Microwave and Optical Technology Letters **55**, 2877 (2013).

[17] A. Tomita and K. Nakamura, Optics Letters **27**, 1827 (2002).

[18] H. Hashimoto, A. Tomita and A. Okamoto, Proc. SPIE **8997**, 899709 (2014).

[19] J. C. Campbell, S. Wenlu, L. Zhiwen, M. A. Itzler and J. Xudong, IEEE Journal of Quantum Electronics **48**, 1505 (2012).

[20] Z. Lu, W. Sun, Q. Zhou, J. Campbell, X. Jiang and M. A. Itzler, Optics Express **21**, 16716 (2013).

[21] M. Itzler, R. Ben-Michael, C.-F. Hsu, K. Slomkowski, A. Tosi, S. Cova, F. Zappa and R. Ispasoiu, Journal of Modern Optics **54**, 283 (2007).

[22] X. M. Zhang, C. Liang, G. Liu, D. Y. Fan, P. Lang, Z. B. Sun, H. Q. Ma, R. Zhang and M. Lei, Journal of Modern Optics **60**, 983 (2013).